Reduction of Transmitter B_1 Inhomogeneity With Transmit SENSE Slice-Select Pulses

Zhenghui Zhang,[1] Chun-Yu Yip,[2,3] William Grissom,[4] Douglas C. Noll,[2–4] Fernando E. Boada,[1,5] and V. Andrew Stenger[6*]

Parallel transmitter techniques are a promising approach for reducing transmitter B_1 inhomogeneity due to the potential for adjusting the spatial excitation profile with independent RF pulses. These techniques may be further improved with transmit sensitivity encoding (SENSE) methods because the sensitivity information in pulse design provides an excitation that is inherently compensated for transmitter B_1 inhomogeneity. This paper presents a proof of this concept using transmit SENSE 3D tailored RF pulses designed for small flip angles. An eight-channel receiver coil was used to mimic parallel transmission for brain imaging at 3T. The transmit SENSE pulses were based on the fast-k_z design and produced 5-mm-thick slices at a flip angle of 30° with only a 4.3-ms pulse length. It was found that the transmit SENSE pulses produced more homogeneous images than those obtained from the complex sum of images from all receivers excited with a standard RF pulse. Magn Reson Med 57:842–847, 2007. © 2007 Wiley-Liss, Inc.

Key words: brain imaging; B_1 inhomogeneity; transmit SENSE; parallel transmitters; tailored RF pulses

The advantages of MRI at high static magnetic field strengths ($B_0 \geq 3$T) include an increased signal-to-noise ratio (SNR) (1) and increased BOLD functional MRI (fMRI) contrast (2). A confound at high B_0, however, is increased image artifact from RF field (B_1) inhomogeneity (3,4). The two factors that produce B_1 inhomogeneity are the shorter RF wavelength, which is further shortened by the dielectric properties of tissue, and the attenuation of RF amplitude due to tissue conductivity (5,6). These artifacts typically appear in the images as regions of increased and decreased brightness at 3T (7). B_1 inhomogeneity can even produce regions with no signal at ultrahigh fields (8). The result of B_1 inhomogeneity can be a loss of image contrast and an improper measure of the spin density.

[1]Department of Bioengineering, University of Pittsburgh, Pittsburgh, Pennsylvania, USA.

[2]Department of Electrical Engineering, University of Michigan, Ann Arbor, Michigan, USA.

[3]Department of Computer Science, University of Michigan, Ann Arbor, Michigan, USA.

[4]Department of Biomedical Engineering, University of Michigan, Ann Arbor, Michigan, USA.

[5]Department of Radiology, University of Pittsburgh, Pittsburgh, Pennsylvania, USA.

[6]Department of Medicine, University of Hawaii, Honolulu, Hawaii, USA.

Grant sponsor: National Institutes of Health; Grant numbers: R01MH66066; R21DA015900.

*Correspondence to: V. Andrew Stenger, Ph.D., UH-QMC Magnetic Resonance Research Center, Department of Medicine, John A. Burns School of Medicine, University of Hawaii, 7th Floor, 1356 Lusitana Street, Honolulu, HI 96813-2427. E-mail: stenger@hawaii.edu

Received 22 March 2006; revised 29 December 2006; accepted 31 January 2007.

DOI 10.1002/mrm.21221
Published online in Wiley InterScience (www.interscience.wiley.com).

Numerous methods have been proposed to mitigate B_1 inhomogeneity artifacts. These include specially designed coils (9,10), adiabatic pulses (11), image postprocessing (12), and small-tip-angle tailored RF (TRF) pulses (13–15). TRF pulse techniques have the advantage of being able to compensate for the transmit B_1 inhomogeneity using a predetermined spatial excitation. More recently, it was shown that "B_1 shimming" can be performed using multiple transmitters (16–18). A homogeneous slice can be achieved by adjusting the magnitude and phase on each transmitter channel until a uniform composite excitation is obtained. The disadvantage of this approach is that there is no straightforward way to relate the observed inhomogeneity to the required RF pulse parameters for each transmitter.

There is currently much interest in transmit sensitivity encoding (SENSE) techniques because of the potential for reduced pulse lengths and power management (19,20). Transmit SENSE techniques were recently validated with parallel transmit hardware in phantoms using 2D RF pulses in a spin-echo sequence (21), and a recent study proposed that transmit SENSE techniques can be used to reduce transmit B_1 inhomogeneity (22). The hypothesis is that the transmit SENSE formalism provides a general approach for designing TRF pulses that are compensated for transmit B_1 inhomogeneity because the transmitter coil sensitivities are inherent in the pulse design. The purpose of this paper is to provide a proof of this concept using a practical three-dimensional (3D) TRF pulse. Due to a lack of transmit SENSE hardware, a pseudo transmit SENSE approach is implemented using a body coil for transmission and an array coil for reception. The technique is demonstrated to reduce the transmit B_1 inhomogeneity in 5-mm-thick slices using 4.3-ms-long pulses in phantom and human brains images at 3T.

THEORY

Assuming small flip angles, the composite spatial excitation profile $w(\mathbf{r})$ from N simultaneous 3D TRF pulses can be written as the sum of the individual excitation profiles $w_n(\mathbf{r})$ produced by each pulse:

$$w(\mathbf{r}) = \sum_{n=1}^{N} w_n(\mathbf{r}) = p(z) \sum_{n=1}^{N} q_n(x,y). \quad [1]$$

Here n represents an array element, and we assume that the excitation is separable such that $p(z)$ is the excitation profile along the slice-select direction, which we will make identical for all pulses. The term $q_n(x,y)$ represents the in-plane excitation profile, which we have the freedom

to control with the pulse design provided that we have adequate excitation *k*-space sampling. The magnetization $M(\mathbf{r})$ that gets excited in the object will then be

$$M(\mathbf{r}) = M_0 p(z) \sum_{n=1}^{N} \alpha_n(x,y) q_n(x,y), \quad [2]$$

where $\alpha_n(x,y)$ is the transmitter sensitivity, or equivalently the transmit B_1 inhomogeneity, and M_0 is the equilibrium magnetization. Here we assume that any variation along the slice-select direction is negligible. If we desire a uniform image with a slice thickness defined by the width of $p(z)$, then

$$\sum_{n=1}^{N} \alpha_n(x,y) q_n(x,y) = \text{const.} = 1. \quad [3]$$

This can be rewritten using the Fourier transform $Q_n(k_x,k_y)$ of the in-plane excitation profile $q_n(x,y)$:

$$\sum_{n=1}^{N} \alpha_n(x,y) \int Q_n(k_x,k_y) e^{-ik_x x - ik_y y} dk_x dk_y = 1. \quad [4]$$

This equation is recognizable as the image domain transmit SENSE equation (23), with the restriction that the resultant magnetization must be constant (i.e., one). This equation can be rewritten as a matrix equation:

$$\alpha Q = 1 \quad [5]$$

and approximate solutions for Q can be obtained by least-squares minimization:

$$Q_{app} = \underset{Q}{\text{argmin}} \|1 - \alpha Q\|^2. \quad [6]$$

The requirements of the above theoretical arguments are easily met using the fast-k_z pulse design (15), which consists of a train of slice-select subpulses of shape $P(k_z)$ (which is the Fourier transform of $p(z)$) separated by phase-encoding blips in *x* and *y*. This design is optimal if thin slices are required along *z* and minimal excitation resolution in *x*-*y* is desired. This is the case for a slice-select pulse that needs to compensate a smoothly varying transmitter B_1 inhomogeneity. The use of phase encoding in *x* and *y* allows for a large degree of freedom in choosing sampling trajectories. Figure 1 shows the k_x-k_y sampling used for the pulses in this work, which was chosen to be hexagonal for optimal alias placement. Each point corresponds to the location of a slice-select subpulse, and the sign corresponds to the polarity of the *z*-gradient. Seven subpulses were used in this trajectory. Figure 1 also provides a definition for the transmit SENSE reduction factor *R*, which can be used to scale the phase-encoding blip area to increase the excitation resolution at the expense of a reduced excitation FOV. Normally $R > 1$ would result in an aliased excitation profile; however, the inclusion of the transmitter spatial sensitivities in Eq. [4] allows for reduced k_x-k_y sampling.

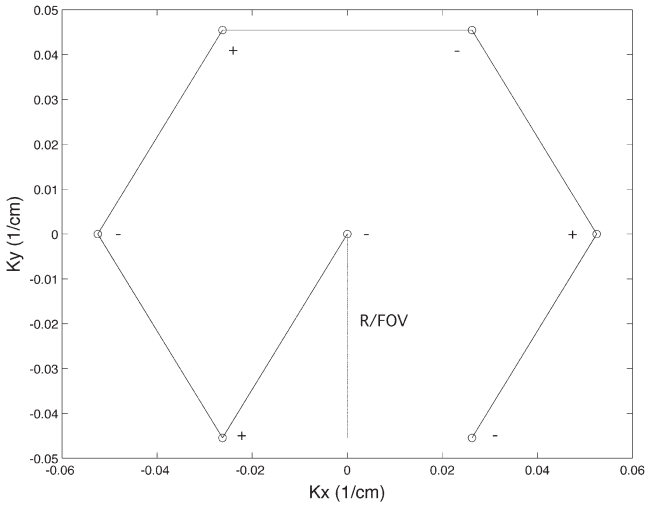

FIG. 1. Diagram of the *k*-space trajectory in the transverse plane used for the transmit SENSE fast-k_z 3D TRF pulses. Phase-encoding blips in *x* and *y* are used to traverse the k_x-k_y plane. A slice-select subpulse is applied along *z* at each point. The sign gives the polarity of the slice-select *z*-gradient.

Due to a lack of parallel transmit hardware, the scanner's standard transmit body coil and multichannel receiver head coil can be used to perform a "pseudo transmit SENSE." This work-around assumes linearity between the reconstructed images, transmit sensitivity, and receive sensitivity, which is reasonable for small tip angles. The procedure begins with first measuring the receive sensitivities $c_n(x,y)$ for *N* receiver coils. *N* unique 3D RFT pulses are then constructed using Eq. [4] with $\alpha_n(x,y)$ replaced by $c_n(x,y)$. Each RF pulse is then sequentially transmitted with the body coil and received with only the phased-array element corresponding to that pulse such that *N* unique complex images are acquired. The final image $I(\mathbf{r})$ is obtained by summing all *N* complex images generated by the different pulses (this mimics the "simultaneous transmission"). Any slice profile aliasing due to reduced pulse lengths (i.e., undersampling) will be canceled by the complex summation. This process can be written as

$$\begin{aligned} I(r) &= \sum_{n=1}^{N} C_n(x,y) M_n(\mathbf{r}) \\ &= M_0 p(z) \alpha(x,y) \sum_{n=1}^{N} c_n(x,y) q_n(x,y) \\ &= M_0 p(z) \alpha(x,y) \sum_{n=1}^{N} c_n(x,y) \int Q_n(k_x,k_y) e^{-ik_x x - ik_y y} dk_x dk_y \end{aligned} \quad [7]$$

Note the similarity of this equation to Eq. [4]. A second assumption made is that there exists a transmit array with transmit sensitivities similar to the receive sensitivities of the coil array used in this work. Although the details of transmit coil construction are beyond the scope of this

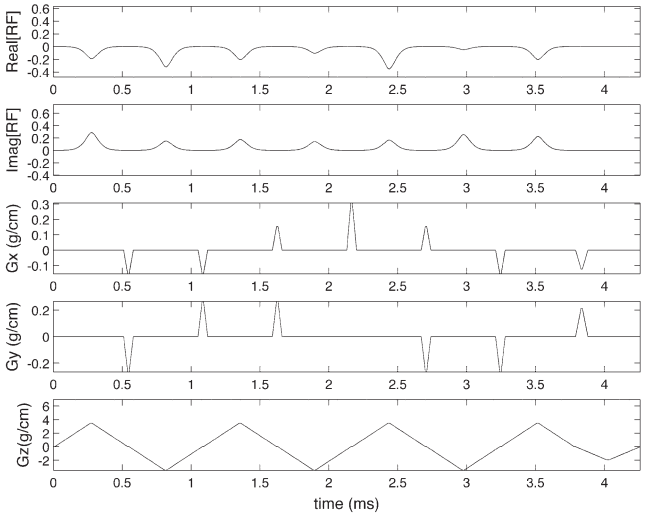

FIG. 2. Example of one of eight 4.3-ms-long transmit SENSE fast-k_z 3D TRF pulses used in the imaging experiments. The rows from top to bottom are the real and imaginary parts of the RF, and the *x*, *y*, and *z* gradients.

work, recent work using true transmit SENSE hardware supports this assumption, as well as that of linearity (21).

MATERIALS AND METHODS

The transmit SENSE 3D TRF pulses were designed for use on a Siemens 3T Trio scanner (Siemens Medical Systems, Erlangen, Germany). The gradient slew rate and peak were 200 T/m/s and 40 mT/m. The scanner's standard transmit body coil and eight-channel receiver head coil were used to mimic transmit SENSE as described above. The receive sensitivity maps $c_n(x,y)$ were determined using array images and a body coil image (each acquired with the fast low-angle shot (FLASH) sequence described below) in an iterative fitting method (24). The iterative technique removes the discontinuities in the sensitivity maps at the object edges, producing a smoother excitation. Once the sensitivity maps were found for the slices of interest, the amplitudes $Q_n(k_x,k_y)$ of each subpulse were determined from Eq. [7] using a conjugate-gradient technique. As described above and in Fig. 1, the pulses consisted of seven subpulses, yielding a total length of 4.3 ms with an excitation resolution of 7.3 cm ($R = 1$) or 4.8 cm ($R = 1.5$) over a 22-cm excitation FOV. The slice-select profile $p(z)$ was chosen to be Gaussian with a half width of 5 mm. All of the pulse construction programs were executed using Matlab (The Mathworks, Natick, MA, USA), which took approximately 1–2 s. An example of a transmit SENSE 3D TRF pulse for one coil is shown in Fig. 2.

A standard 2D FLASH sequence with fat saturation and sequence parameters TE = 15 ms, TR = 300 ms, FA = 30°, and matrix size = 128 × 128 was used for acquisition. These parameters were chosen such that a single slice could be acquired rapidly with sufficient contrast and SNR. The sequence could implement either the 3D TRF pulses or a standard slice-select pulse with the same $p(z)$ and flip angle. Final images from the standard pulse were similarly obtained from a complex summation of the individual coil images. The scanner reconstruction performed a low-resolution phase correction on the complex image from each receiver such that any additional image phase from the coil geometry was removed. This combination was chosen to mimic a simultaneous excitation with multiple transmitters without transmit SENSE. An 18-cm-diameter uniform spherical phantom (12.5 mM NAA, 10 mM Cre, 3 mM Cho, 5 mM actate, 12.5 mM Glu, and 7.5 mM mI, pH 7.2, 0.1% Magnevist) and five normal adult human subjects were scanned. The human subjects were studied under approval of the University of Hawaii and Queens Medical Center Joint Institutional Review Board.

In the human scans we assumed that the body coil had a uniform transmit profile $\alpha(x,y) = 1$. In one of the phantom scans, however, we included an analytical estimate for the body coil sensitivity:

$$\alpha(x,y) = 1 - Ae^{-\pi[(x/x_0)^2+(y/y_0)^2]}. \quad [8]$$

This equation represents a 2D Gaussian subtracted from unity to compensate for the increased magnitude in the image center due to body coil inhomogeneity. The parameters A, x_0, and y_0 were used to adjust the magnitude and width of the 2D Gaussian function in an ad hoc fashion by visual inspection of the images. This was done to demonstrate that a complete correction requires consideration for both transmit and receive B_1 inhomogeneity.

Two methods were used to analyze B_1 inhomogeneity in the resultant slices. The first approach constructed histograms of the image magnitude distributed among all of the pixels in an image (25). A smaller width of the histogram is indicative of the degree of magnitude uniformity. The width was determined by a least-squares fit of the histograms with a Gaussian function $g(m)$:

$$g(m) = ae^{-\frac{(x-b)^2}{c^2}}, \quad [9]$$

where m is the bin number, and the parameters a, b, and c were determined by the fitting procedure. The full width

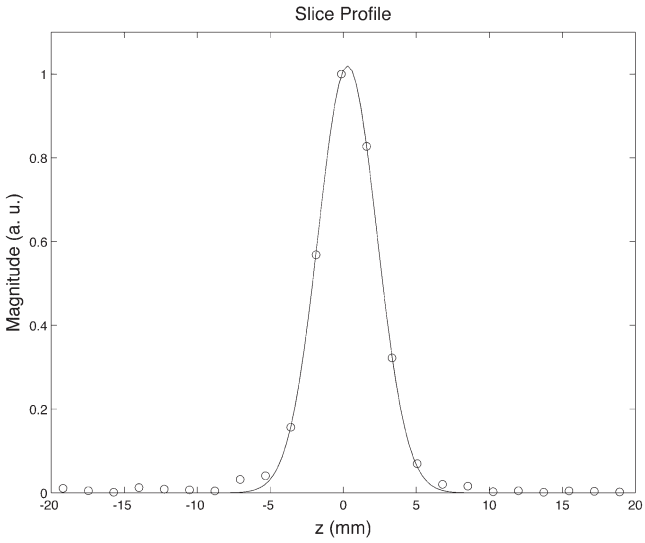

FIG. 3. The circles show the experimental slice profile obtained from a transmit SENSE fast-k_z 3D TRF pulse in a uniform phantom. The solid line shows a Gaussian fit with a half width of 4.7 mm.

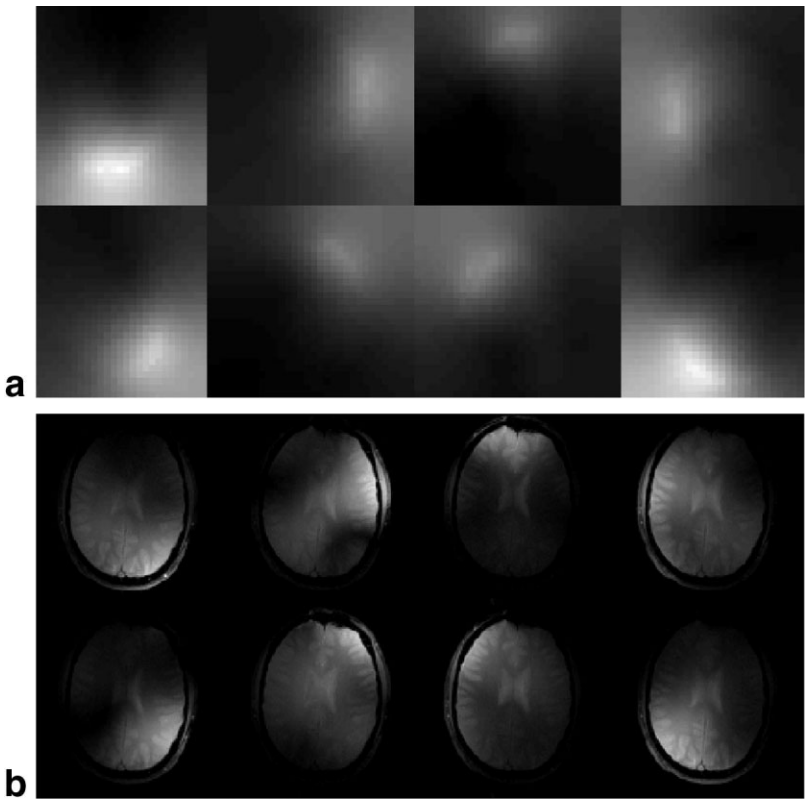

FIG. 4. **a:** Example of the eight estimated sensitivity maps for a human brain slice. **b:** The corresponding eight individual coil magnitude images acquired using an $R = 1.5$ transmit SENSE pulse tailored for that coil. The complex sum of the eight images is shown by the middle image in Fig. 5b.

half at maximum (FWHM) of the histograms was calculated with

$$\mathrm{FWHM} = 2c\sqrt{\ln(2)}. \quad [10]$$

The second method was to calculate the normalized standard deviation (SD/mean) of all of the pixel magnitudes in a given slice, excluding the region outside brain. A larger SD is indicative of a large degree of B_1 inhomogeneity. The data analyses and statistical methods were all performed using Matlab.

RESULTS

Figure 3 shows the experimental slice profile from a transmit SENSE 3D TRF pulse taken in the uniform phantom. Also shown is a Gaussian fit to the data that yields a slice thickness of 4.7 mm, in good agreement with the desired 5 mm. Figure 4a shows example sensitivity maps for one slice in a subject. Figure 4b shows the corresponding eight individual coil images acquired using an $R = 1.5$ pulse (the middle slice in Fig. 5b shows the complex sum of these eight images).

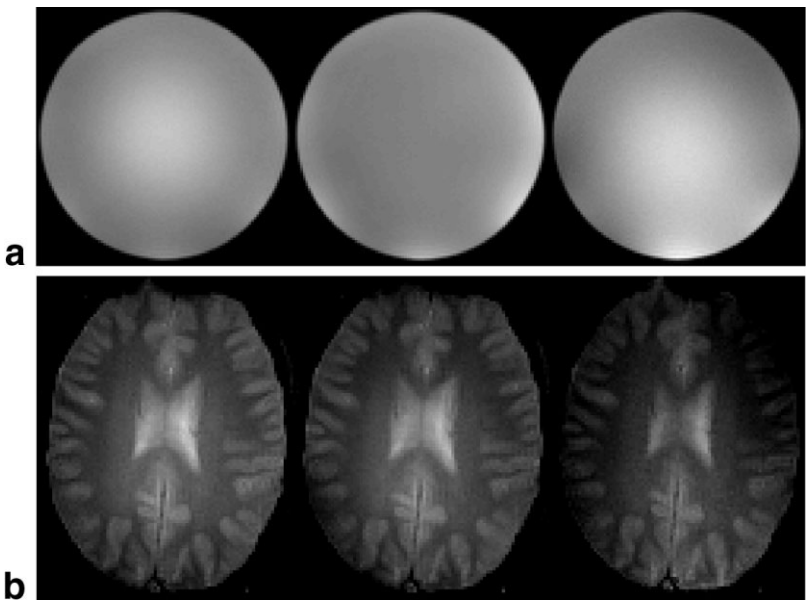

FIG. 5. **a:** Images of a uniform phantom excited with an $R = 1$ transmit SENSE pulse without (left) and with (middle) the body coil sensitivity correction, and an image obtained from complex summation using a standard pulse (right). **b:** Brain images obtained using $R = 1$ (left) and $R = 1.5$ (middle) transmit SENSE pulses, and an image obtained using the complex sum and standard pulse (right).

Figure 5a shows images of the uniform phantom excited with an $R = 1$ transmit SENSE pulse without (left) and with (middle) the additional correction for the body coil sensitivity given by Eq. [8]. The image on the right shows the result of complex summation using the standard pulse. All of the images are shown with the same window and level. Visual inspection shows that the image acquired with the standard pulse is the most inhomogeneous. Note that the inhomogeneity from the body coil is also apparent in the left and right images and was corrected in the middle image. Although the transmit SENSE technique is focused on reducing transmitter B_1 inhomogeneity, this demonstrates that both transmitter and receiver B_1 inhomogeneities need to be considered. Figure 5b shows a comparison of a brain image obtained from one subject using $R = 1$ (left) and $R = 1.5$ (middle) transmit SENSE pulses, as well an image obtained using the complex sum and standard pulse (right). All of the images are shown with the same window and level. By visual inspection, the images acquired with the transmit SENSE pulses are more uniform than the image obtained using the standard pulse.

Figure 6a shows histograms of the distributions of pixel magnitudes in the phantom images shown in Fig. 5a. The half widths of the histograms were measured to be 7.9, 3.6, and 2.3 for the standard pulse and the transmit SENSE pulse without and with the body coil sensitivity compensation. Figure 6b shows histograms of the distributions of pixel magnitudes in the brain images shown in Fig. 5b. The images acquired with the transmit SENSE pulses have narrower histograms. Note that although no additional aliasing is seen in the image acquired with the $R = 1.5$ pulse, the additional excitation resolution provided by the pulse (4.9 cm) did not produce any noticeable improvement in image uniformity. The FWHM of histograms and the SD/mean measurements of slices obtained in all five subjects are listed in Table 1. Both the FWHM and SD/mean measurements of the transmit SENSE pulse images are smaller than the corresponding slices generated using the standard pulse. A *t*-test was performed to compare the FWHM and SD/mean of the transmit SENSE slices with those of the slices generated with the standard pulse. The subsequent *P*-values all indicate that the differences in means of these parameters are statistically significant.

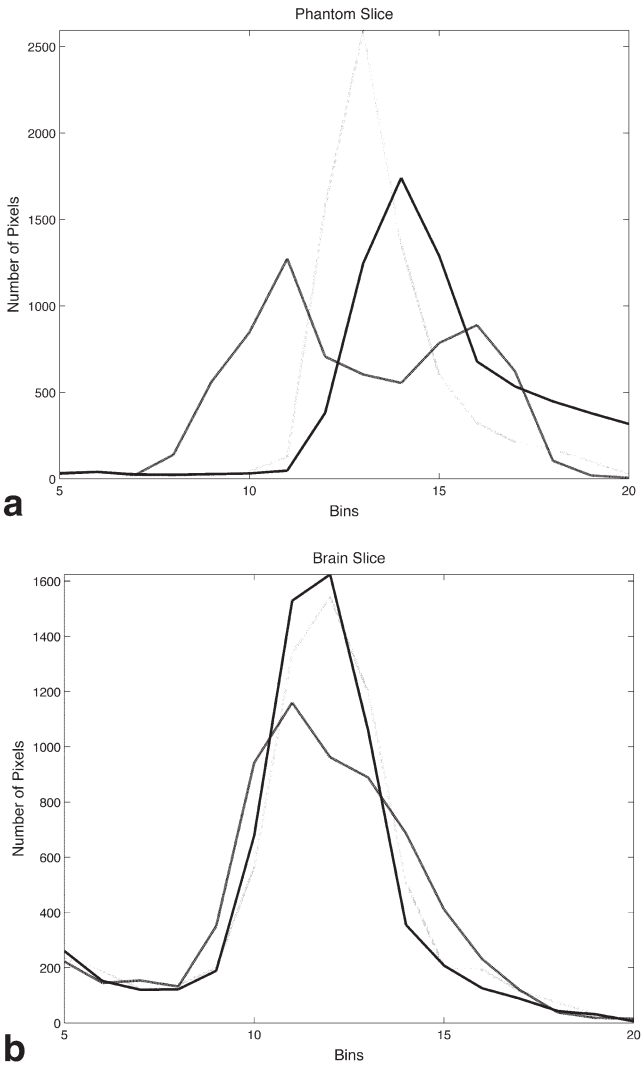

FIG. 6. **a:** Histograms of pixel magnitudes from the phantom images shown in Fig. 5a. The black, light gray, and gray lines are from the left, middle, and right images, respectively. **b:** Histograms of pixel magnitudes from the phantom images shown in Fig. 5b. The black, gray, and light gray lines are from the left, middle, and right images, respectively.

DISCUSSION AND CONCLUSIONS

This work presents a theoretical description of the inherent B_1 inhomogeneity compensation property of the transmit SENSE technique, as well as a demonstration using a practical slice-select 3D TRF pulse implementation. We also devised a work-around to mimic transmit SENSE using a phased-array receiver and complex summation. This requires an assumption of linearity as well as the existence of a transmit array with sensitivities similar to those of a typical receiver array. These assumptions appear to be reasonable, as demonstrated in a previous work that compared parallel transmission to complex summation (21). We found that the transmit SENSE pulses at 3T provided a statistically significant improvement in image uniformity compared that obtained using a standard pulse. As in our previous work (15), the fast-k_z pulse design provided a practical 3D TRF implementation for a 5-mm-thick slice. We found that 4.3-ms-long pulses with a 7.3-cm excitation resolution ($R = 1$) and 22-cm excitation FOV were adequate at 3T. Furthermore, multiple slices in a single subject should present no difficulty. In this study we used flip angles of only 30°; however, an investigation of larger flip angles will be conducted in the future.

The limitations of this work include the lack of a demonstration using parallel transmission hardware. Only a few centers will be equipped with such systems for the near future. As such, we were unable to perform a true comparison of transmit SENSE with simultaneous transmission ("B_1 shimming") using pulses with optimized magnitudes and phases. It may be that B_1 shimming techniques can offer equivalent image uniformity; however, our results indicate that transmit SENSE pulses show promise and are reasonably practical to implement. It is also possible that a single pulse used with multiple transmitters, or the previously described pulse (15) using a volume coil are just as effective at compensating for the

Table 1
Full Width at Half Maximum (FWHM) of Histograms as Well as Standard Deviations (SDs) Divided by the Mean of the Image Magnitudes of the Human Brain Slices*

	FWHM		SD/mean	
	Transmit SENSE	Standard pulse	Transmit SENSE	Standard pulse
Slice 1	0.16	0.22	0.13	0.17
Slice 2	0.15	0.22	0.13	0.16
Slice 3	0.15	0.27	0.12	0.16
Slice 4	0.17	0.23	0.15	0.19
Slice 5	0.15	0.26	0.15	0.18
P-value	0.0002		0.003	

*Also shown are *P*-values from a *t*-test between the slices excited using the transmit SENSE pulse (R = 1) and the standard pulse.

transmitter B_1 inhomogeneity. Multiple transmitters may not be absolutely necessary. The use of one transmitter or one pulse would simplify implementation; however, it would not be possible to obtain reduction factors or other benefits of multiple transmitters, such as power management.

Although we show in Fig. 5a that both transmitter and receiver inhomogeneity may be incorporated into the pulse design, this was done only for demonstrative purposes. We believe that the receiver inhomogeneity would be better addressed during reconstruction. The use of parallel transmission has also been proposed to address the problems of ultrahigh-field imaging, such as at 7T (17). Although our demonstration was performed at 3T, there is no theoretical reason to suggest that some implementation of transmit SENSE would not have a possible role at ultrahigh fields. The use of ultrahigh fields, as well as the effects of power absorption and large flip angles, will need to be evaluated before final judgment can be made.

REFERENCES

1. Edelstein WA, Glover GH, Hardy CJ, Redington RW. The intrinsic signal-to-noise ratio in NMR imaging. Magn Reson Med 1986;3:604–618.
2. Ogawa S, Lee T, Nayak A, Glynn P. Oxygenation-sensitive contrast in magnetic resonance image of rodent brain at high magnetic fields. Magn Reson Med 1990;14:68–78.
3. Bottomley P, Andrews E. RF magnetic field penetration, phase shift and power dissipation in biological tissue: implications for NMR imaging. Phys Med Biol 1978;23:630–643.
4. Glover GH, Hayes CE, Pelc NJ, Edelstein WA, Mueller OM, Hart HR, Hardy CJ, O'Donnell M, Barber WD. Comparison of linear and circular polarization for magnetic resonance imaging. J Magn Reson 1985;64:255–270.
5. Yang QX, Wang J, Zhang X, Collins CM, Smith MB, Liu H, Zhu XH, Vaughan JT, Ugurbil K, Chen W. Analysis of wave behavior in lossy dielectric samples at high field. Magn Reson Med 2002;47:982–989.
6. Collins CM, Liu W, Schreiber W, Yang QX, Smith MB. Central brightening due to constructive interference with, without, and despite dielectric resonance. J Magn Reson Imaging 2005;21:192–196.
7. Jin J, Chen J. On the SAR and field inhomogeneity of birdcage coils loaded with the human head. Magn Reson Med 1997;38:953–863.
8. Ibrahim TS, Lee R, Abduljalil AM, Baertlein BA, Robitaille PM. Dielectric resonances and B(1) field inhomogeneity in UHFMRI: computational analysis and experimental findings. Magn Reson Imaging 2001;19:219–226.
9. Alsop D, Connick T, Mizsei G. A spiral volume coil for improved RF field homogeneity at high static magnetic field strength. Magn Reson Med 1998;40:49–54.
10. Vaughan J, Adriany G, Garwood M, Yacoub E, Duong T, DelaBarre L, Anderson P, Ugurbil K. Detunable transverse electromagnetic (TEM) volume coil for high-field NMR. Magn Reson Med 2002;47:990–1000.
11. Staewen R, Johnson A, Ross B, Parrish T, Merkle H, Garwood M. 3-D FLASH imaging using a single surface coil and a new adiabatic pulse, BIR-4. Invest Radiol 1990;25:559–567.
12. Cohen MS, DuBois RM, Zeineh MM. Rapid and effective correction of RF inhomogeneity for high field magnetic resonance imaging. Hum Brain Mapp 2000;10:204–211.
13. Deichmann R, Good C, Turner R. RF inhomogeneity compensation in structural brain imaging. Magn Reson Med 2002;47:398–402.
14. Saekho S, Boada FE, Noll DC, Stenger VA. A small tip angle 3D tailored RF slab-select pulse for reduced B1 inhomogeneity at 3T. Magn Reson Med 2005;53:479–484.
15. Saekho S, Yip C-P, Noll DC, Boada FE, Stenger VA. A fast-kz 3D tailored RF pulse for reduced B1 inhomogeneity. Magn Reson Med 2006;55:719–724.
16. King SB, Duensing GR, Varosi S, Peterson D, Molyneaux DA. A four channel transceive phased array head coil for 3T. In: Proceedings of the 9th Annual Meeting of ISMRM, Glasgow, Scotland, 2001 (Abstract 12).
17. Adriany G, Van de Moortele PF, Wiesinger F, Moeller S, Strupp JP, Andersen P, Snyder C, Zhang X, Chen W, Pruessmann KP, Boesiger P, Vaughan T, Ugurbil K. Transmit and receive transmission line arrays for 7 Tesla parallel imaging. Magn Reson Med 2005;53:434–445.
18. Collins CM, Liu W, Swift BJ, Smith MB. Combination of optimized transmit arrays and some receive array reconstruction methods can yield homogeneous images at very high frequencies. Magn Reson Med 2005;54:1327–1332.
19. Zhu Y. Parallel excitation with an array of transmit coils. Magn Reson Med 2004;51:775–784.
20. Katscher U, Bornert P, Leussler C, van den Brink J. Transmit SENSE. Magn Reson Med 2003;49:144–150.
21. Ullmann P, Junge S, Wick M, Seifert F, Ruhm W, Hennig J. Experimental analysis of parallel excitation using dedicated coil setups and simultaneous RF transmission on multiple channels. Magn Reson Med 2005;54:994–1001.
22. Stenger V, Zhang Z, Yu S, Boada F. B1 Inhomogeneity reduction with transmit SENSE. In: Proceedings of the 2nd International Workshop on Parallel MRI, Zurich, Switzerland, 2004. p 94.
23. Grissom W, Yip CY, Zhang Z, Stenger VA, Fessler JA, Noll DC. Spatial domain method for the design of RF pulses in multicoil parallel excitation. Magn Reson Med 2006;56:620–629.
24. Fessler JA. Penalized weighted least-squares image reconstruction for positron emission tomography. IEEE Trans Med Imaging 1994;13:290–300.
25. Wang J, Qiu M, Yang QX, Smith MB, Constable RT. Measurement and correction of transmitter and receiver induced nonuniformities in vivo. Magn Reson Med 2005;53:408–417.
26. Van de Moortele PF, Akgun C, Adriany G, Moeller S, Ritter J, Collins CM, Smith MB, Vaughan JT, Ugurbil K. B(1) destructive interferences and spatial phase patterns at 7 T with a head transceiver array coil. Magn Reson Med 2005;54:1503–1518.